Highly performing graphene-based field effect transistor for the differentiation between mild-moderate-severe myocardial injury

Teresa Rodrigues, Vladyslav Mishyn, Yann R. Leroux, Laura Butruille, Eloise Woitrain, Alexandre Barras, Patrik Aspermair, Henri Happy, Christoph Kleber, Rabah Boukherroub, et al.

Highly performing graphene-based field effect transistor for the differentiation between mild-moderate-severe myocardial injury

Teresa Rodrigues,[1,2] Vladyslav Mishyn,[1,2] Yann R. Leroux,[3] Laura Butruille,[4] Eloise Woitrain,[4] Alexandre Barras,[1] Patrik Aspermair,[2] Henri Happy,[1] Christoph Kleber,[5] Rabah Boukherroub,[1] David Montaigne,[4] Wolfgang Knoll,[5]* and Sabine Szunerits[1*]

[1] *Univ. Lille, CNRS, Centrale Lille, Univ. Polytechnique Hauts-de-France, UMR 8520 - IEMN, F-59000 Lille, France*

[2] *AIT Austrian Institute of Technology GmbH, Biosensor Technologies, 3430 Tulln, Austria*

[3] *Univ. Rennes, CNRS, ISCR – UMR 6226, Campus de Beaulieu, F-35000 Rennes, France*

[4] *Univ. Lille, Inserm, CHU Lille, Institut Pasteur de Lille, U1011- EGID, F-59000 Lille, France*

[5] *Department of Scientific Coordination and Management, Danube Private University, A-3500 Krems, Austria*

Abstract

Cardiovascular diseases result in millions of deaths around the globe, many of which could have been avoided if identified at an early stage. Preventive cardiovascular disease diagnostics plays a vital role reducing the critical fatality rate by allowing to take timely necessary precautions. Here, we demonstrate the exceptional properties of aptamer modified graphene-based FET (GFET) for cardiac troponin I (cTnI) specific sensing in different bodily fluids. Concentration-dependent measurements made with cardiac troponin I (cTnI) on an aptamer/polyethylene glycol (PEG) modified GFET exhibited real-time detection of cTnI from 1-400 pg mL^{-1} in 0.01× phosphate-buffered saline (PBS) solution. The sensor performance is within the clinical important window of 10 pg mL^{-1} to 500 pg mL^{-1}, allowing the differentiation between healthy, and people with low and high risk for myocardial infraction (AMI). Even more important is the very reproducible shift and neglectable leakage current of the individual $I_{DS}V_{GS}$-curves upon contact with cTnI solutions. To further evaluate the applicability of the developed point of care device for troponin I sensing in serum, samples of 15 patients with different troponin levels were analysed for their troponin I levels. The 15 patients were grouped

* To whom Correspondence should be send to: wolfgang.knoll@ait.ac.at, sabine.szunerits@univ-lille.fr

according to the magnitude of peri-operative myocardial injury as assessed by the clinical hs-cTnT assay into mild (cTnT <15 pg mL^{-1}), moderate (15 pg mL^{-1}> c-TnT <500 mL^{-1}) and severe (cTnT >500 pg/mL), cases. The GFET sensor allowed to categorise all the 15 samples correctly and corresponding to 3 troponin zones (respectively, low, medium and high). While indeed a larger patient sample collection is required for clinical assessments, these data seem highly promising.

Keywords: Graphene-based field effect transistor, aptamer, cardiac troponin I, biosensor.

Introduction

Over more than 10 years, cardiac troponin (cTn) has become the preferred serum biomarker for diagnosis and rule out of acute myocardial infarction (AMI) [1]. Significant improvements in cTn assays with regards to analytical sensitivity have resulted in the availability of highly sensitive cTnI (hs-cTnI) assays that enable detection of cTnI values that are ten-fold lower than the 40 pg mL^{-1} cut-off for detection of myocardial ischemia. Most importantly, this hs-cTnI assay generation [2] can finally differentiate healthy patients from patients with myocardial ischemia and early necrosis due to their adapted detection limit of 1.5 pg mL^{-1} (LOQ=2.5 pg mL^{-1}). To reach this sensitivity using immunoassays, patient serum samples are mixed with solid phase magnetic beads coated with monoclonal antibodies to capture the cTnI. Addition of anti-human recombinant sheep Fab fragments linked to bovine serum albumin labelled with a chemiluminescent signal producing substrate, acridinium ester, allowed cTnI quantification in about 20 min [3]. Troponin diagnostics thus evolved from a test to diagnose of AMI to one that allows early detection of cardiac injury.

Highly-sensitive point-of-care testing (POCT) assays represent the next challenge for troponin detection. As several clinical laboratories are unable to meet the recommended one-hour reporting time for troponin results, a POCT device that tests serum samples and is implemented within the emergency department can reduce substantially the detection time. We believe that the format of graphene-based field effect transistor (GFET) [4-11] is ideally adapted for opening up opportunities for cTnI point of care testing. The uniqueness of graphene as the semiconductor channel in biosensors is linked to its excellent electrical properties (e.g. high mobility, high transfer kinetics, high conductivity), biocompatibility, chemical inertness and high sensitivity to near surface charges and electric fields [9, 11]. The sensing principle in these electrical devices is based on changes of the electrical conductance of the graphene channel upon analyte interaction with its surface. One of the prerequisites of a well-performing GFET biosensor is linked to the use of high-quality graphene with high hole and electron mobilities. Despite the impressive achievements in the electrical performances of GFETs, the reproducibility of sample preparation and maintaining the high mobility after surface modification represent bottlenecks to overcome [12-14]. We have recently demonstrated that CVD graphene-coated interdigitated electrodes functionalized by an ethynylphenyl monolayer via the electrochemical reduction of 4-((triisopropylsilyl)ethynyl)benzene diazonium salt (TIPS-Eth-ArN_2^+) offer an ideal platform for sensing applications where the modified GFET channels hole and electron mobilities reach 1739 ± 376 $cm^2 V^{-1} s^{-1}$ and 1698 ± 536 $cm^2 V^{-1} s^{-1}$,

respectively [15]. Indeed, while a deeper understanding and analysis of the influence of covalent grafting strategy is required, the creation of a functional monolayer might create a continuous path for electrons to flow in one single plane. Furthermore, the diazonium salt might get grafted to specific grain boundaries, edge defects or wrinkles, which then might create an additional conduction path.

In this work, we investigate if this enhanced performance will permit the sensitive cTnI sensing in more complex media other than diluted phosphate-buffered saline (PBS) solution (i.e. patient serum). To enable direct electronic target detection, a single stranded nucleic acid cTnI azide-aptamer with TTT-TCA loop and a CCCTC portion [16, 17] was immobilized onto the graphene transducer channel as a surface receptor (**Figure 1**). The integration of a polyethylene glycol (PEG) chain onto the graphene device next to the cTnI aptamer enabled furthermore, the sensing capabilities of the GFET in physiological solution and patient serum samples [4].

Results

Choosing the right diazonium ligand for improving FET mobility

The GFET used here is based on the wet-transfer of CVD-grown graphene on Cu foils [18] onto interdigitated gold electrodes (IDE) (**Figure 1a**), consisting of 90 electrode pairs of 10 µm in lenght with a 10 µm separation and total surface area of 9.62 mm^2 (r=1.25 mm). To realize bio-detection in physiological solutions, we covalently modified the graphene channel [19, 20] with a troponin-specific aptamer (**Figure 1b**) using a Cu(I) catalysed "click" chemistry between the azide function on the aptamer and ethynyl-modified CVD graphene channels (**Figure 1c**). Ethynyl-terminated graphene was formed in a two-step process: (i) electrochemical reduction of 4-[(triisopropylsilyl)ethylenyl]benzenediazonium tetrafluoroborate (TIPS-Eth-ArN_2^+), (ii) followed by the chemical deprotection of the triisopropylsilyl (TIPS) function. To ensure a good anti-fouling interface and increase the effective screening length in high-ionic solutions, the "click" chemistry was performed in a mixture of an aptamer-N_3 and a PEG-N_3 in a mass ratio of 2:1 (aptamer:PEG). To validate that a 2:1 mixture result in a 2:1 transfer, in a control experiment, a mixture of azide-ferrocene:PEG was applied for the "click" reaction and the amount of surface linked ferrocene moieties was estimated via electrochemical measurements (**Figure S1**). In the absence of PEG, the amount of surface bound ferrocene groups from a solution of 10 µM (a concentration used for the linkage of cTnI aptamer later) was determined as $\Gamma=5.9\times10^{-11}$ mol cm^{-2}. Indeed, at this rather low concentration, no full surface coverage ($\Gamma=4.8\times10^{-10}$ mol cm^{-2}) [21] was achieved. In the case of ferrocene:PEG mixtures using mass

ratios of 2:1 and 1:2, surface coverages $\Gamma=5.1\times 10^{-11}$ mol cm^{-2} and $\Gamma=6.4\times 10^{-12}$ mol cm^{-2} were obtained, respectively. For a ferrocene:PEG mixture 2:1, the linkage was somehow in favour of the ferrocene ligand, while in the case of ferrocene:PEG=1:2, almost no ferrocene ligand could be incorporated onto the sensor chip.

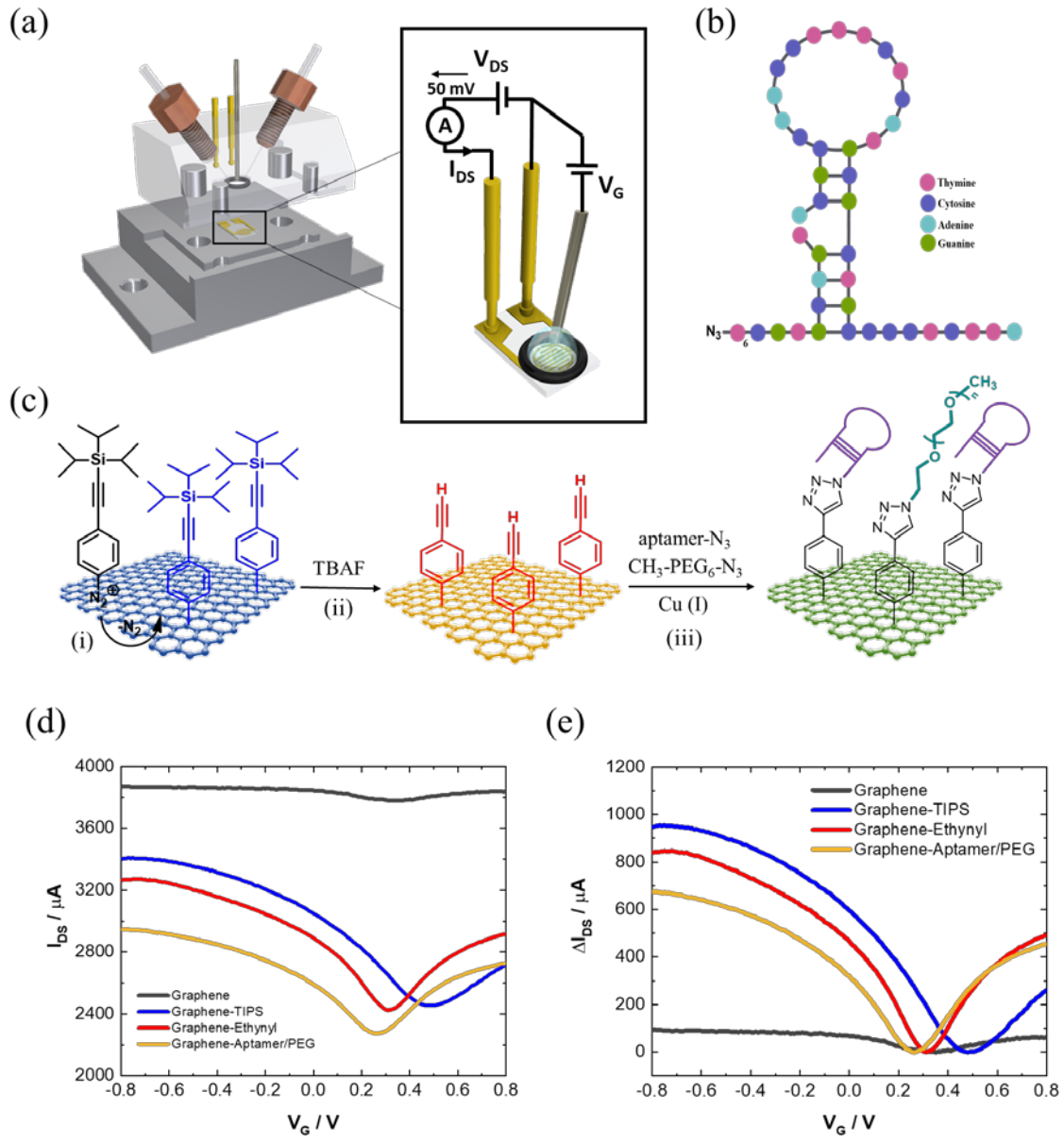

Figure 1: Concept of electrical aptamer sensor for sensing of cTnI in PBS and serum using CVD graphene as a channel material. (a) Graphene-coated interdigitated electrodes covalently modified for cTnI sensing. (b) cTnI azide-aptamer with TTT-TCA loop and a CCCTC portion employed. (c) Scheme of surface modifications steps employed for the integration of a cTnI aptamer: (i) electroreduction of TIPS-Eth-ArN_2^+ followed by (ii) chemical deprotection of the triisopropylsilyl function resulting in ethynyl-terminated graphene channel, and (iii) covalent

binding of azide-terminated ligands in Cu(I)-catalysed "click" chemistry approach. (d) GFET characteristics recorded after each functionalization step (raw data). (e) GFET characteristics recorded after each functionalization step where $\Delta I_{DS} = I_{DS}$-minimum(I_{DS}).

Complete coverage of the drain-source channel with graphene (**Figure S2a**) was achieved by modification of the glass interlayers with trimethoxyphenylsilane (TMPS) to increase the adhesion of graphene. The Raman spectrum of the transferred graphene features bands at 1350 cm^{-1} (defects in the graphene sheet), 1580 cm^{-1} (sp^2-carbon) and 2706 cm^{-1} (secondary D band). Compared to the Raman plot of the initial graphene (**Figure S2b**), the defect band increased only by a factor of 1.32, indicating the preservation of graphene's structure during the wet chemical transfer process.

The drain-source current (I_{DS}) as a function of gate voltage (V_G) **(Figure 1d** for raw data and **Figure 1d** for normalised data) of the different GFET interfaces and the corresponding charge mobilities (**Figure S2d)** clearly show that the charge transfer characteristics of the modified GFET are improved after the diazonium grafting and it furthers remain similar after the covalent attachment of complex biological molecules via "click" chemistry coupling reaction.

The value of capacitance used to calculate the mobility of charge carriers was extrapolated from fitting the leakage current at different scan rates recorded at different applied gate voltages (**Figure S3**). The transistor's channel width (W) and length (L) directly affects the electrical mobility of the device [22] and the mobility is inversely proportional to the aspect ratio W/L (as demonstrated in SI). The initial low mobility is also due to the high W/L ratio ($4.9x10^4$) of our device's architecture, mainly due to the small length and large width attributed to the presence of interdigitated electrodes. The large width will increase the channel surface area defining the number of immobilized bioreceptors at the sensor surface which directly influences the target binding, although it might compromise device's electronic performance. Indeed, our device's channel provides a high W/L ratio when compared to other groups that report W/L ratios of 1 or lower, [23] which will, in turn, reflect in higher carrier mobility. This emphasises the importance of incorporating diazonium-based chemistry on devices that have low mobility at start, which in turn lowers device's sensitivity as a biosensor.

The leakage current (current at the gate electrode) is another important consideration in an electrolyte-gated configuration – an absent effect in traditional configurations, such as back-gated or dielectric-gated FETs. This current is not desirable in any transistor devices, as it

represents a loss of energy, performance, and can interfere with the signal of interest. Svetlova et al., recently tried to comprehend these phenomena on electrolyte-gated FETs using cyclic voltammetry as a complementary method to characterize the processes surrounding the gate electrode [24]. The leakage current is a series of capacitive and faradaic processes that occur on the transistor's surface, possibly attributed to oxygen reduction reactions once a certain potential is applied on the gate electrode. For these oxygen-based reactions to occur, it needs the binding of an oxygen-containing intermediate to a carbon atom in a vicinity of a defect with a subsequent bond cleavage. Thus, graphene defect sites open an area for an oxygen-reduction reaction to happen and so it will be specific for each transistor that carries a unique pattern of defects on its surface. To avoid these side reactions, CVD graphene with low area of defects and oxygen-depleted solutions may be employed, and an extensive positive biasing should be avoided [24]. For these reasons, the leakage current was recorded in all subsequent measurements to ensure that the processes occurring at the vicinity of the channel's surface is mainly (desirably, only) due to the formation of an aptamer-protein complex instead of parallel electrochemical reactions. In this scope, the leakage current was recorded on each modification step (**Figure S2e**), revealing a neglectable contribution of potential side reactions that may occur on the channel surface for most stages. However, after diazonium grafting on the surface there is an increase on the leakage current that may be attributed to the generation of new oxygenated groups on the surface by the activation of defect site areas. While being out of the scope of the present study, technics like X-ray photoelectron spectroscopy (XPS) could be used to determine the composition of the surfaces with grafted diazonium layers, to assess the concentration of the oxygenated groups at the surface, likely responsible for gate leakage.

Influence of transfer characteristics in different biological media

In an electrolyte-gated graphene field-effect transistor, the applied gate voltage leads to an interfacial charge separation between the electrolyte and the graphene channel, a so-called diffusive double-layer. The distance between the two charged layers is called Debye length and this length is highly influenced by the ionic strength of the medium. If the ion concentration in solution is too high, the counter ions may shield the molecular charges that are away from the gate insulator leading to a screening effect, and thus, influencing the transistor's performance as a biosensor. As such, this length should be preferably wide enough to detect the interaction between a sensing probe and a charged analyte. The dependency of the Debye length at a solution/gate interface based on this electrical double layer (EDL) with the ionic strength of the electrolyte solution is expressed by the equation (1):

$$\boldsymbol{\lambda_D = \sqrt{\frac{\varepsilon_0 \varepsilon_r k_B T}{2NAe^2 I}}} \quad (1)$$

where I is the ionic strength of the electrolyte, ε_0 is the permittivity of free space, ε_r is the dielectric constant of the electrolyte, k_B is the Boltzmann constant, T is the absolute temperature, N_A is the Avogadro number, and e is the elementary charge. Furthermore, the ionic strength of an electrolyte I is expressed by the equation (2):

$$\boldsymbol{I = \frac{1}{2} \sum c_i z_i^2} \quad (2)$$

where Σ is the sum of all ions in the electrolyte; i is the total number of ion species; z_i is the number of the charges carried by the ion and c_i is the ion concentration, which determines the ionic strength of an electrolyte. According to equations (1) and (2), the Debye length (λ_D) of a 0.001× PBS solution (I = 0.177 mM) is estimated at about 23 nm, which is larger than those of 0.01× PBS (I = 1.77 mM, λ_D = 7.2 nm), 0.1× PBS (I = 17.7 mM, λ_D = 2.3 nm), and 1× PBS (I = 177 mM, λ_D = 0.72 nm). The lower the electrolyte concentration the smaller the ionic strength and the larger λ_D is (**Figure 2a**). The above statements are valid considering a 2-dimensional plane for surface bound charges at the electrolyte/substrate interface, and seems valid for graphene. Once graphene is functionalized with charged surface receptors, a three-dimensional charge distribution must be considered. This will not compromise the concept of the Debye length dependency on the ionic strength, although it will most likely change the theoretical values derived from equations (1) and (2), and thus a deeper understanding of the whole mechanism as a 3D structure should be evaluated.

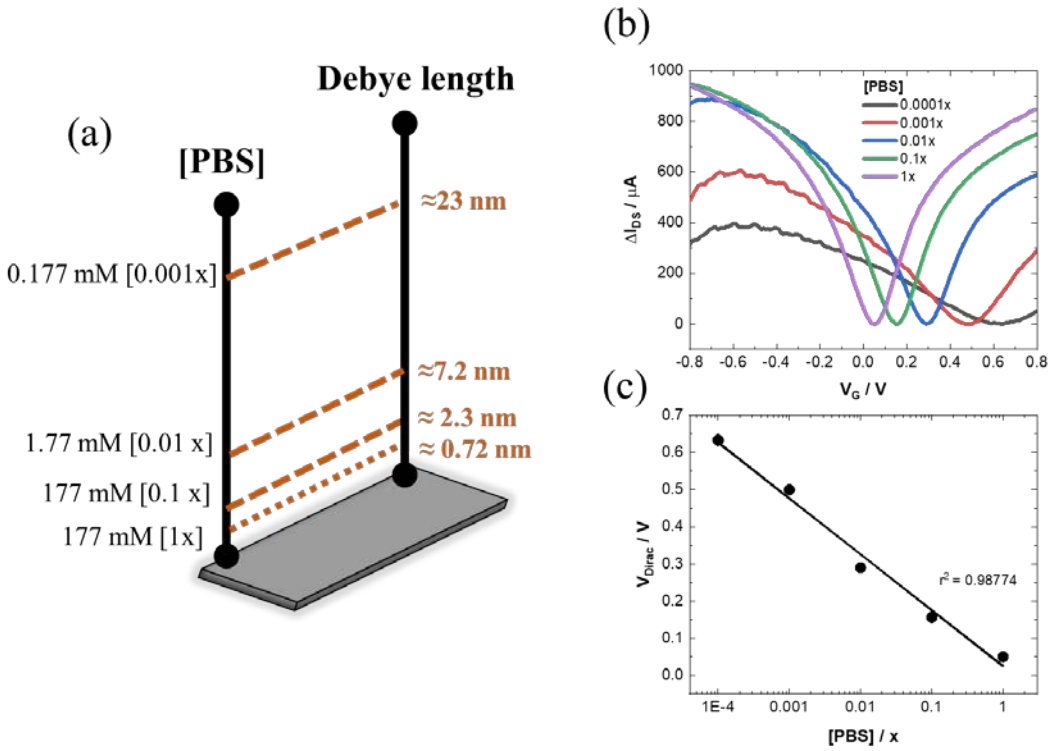

Figure 2: GFET characteristics as a function of PBS concentration where ΔI_{DS} = I_{DS}-minimum(I_{DS}). (a) Correlation of PBS concentration and Debye screening length considering a 2D charge distribution at an unmodified graphene/electrolyte interface. (b) Transfer characteristics of aptamer:PEG modified GFET in PBS at different concentrations. (c) Change of Dirac as a function of PBS concentration with x=1, 0.01, 0.001 and 0.0001, n=3. The current values were treated to start at zero using the equation ΔI_{DS} = I_{DS}-minimum(I_{DS}). See Figures S4 for raw data and gate leakage current values.

To get a better understanding on the operation of the aptamer:PEG modified graphene channel in media of different ionic strengths, graphene transfer characteristics were recorded (**Figure 2b**). Increasing solution ion concentrations induce growing negative charges in graphene and an electrostatic chemical gating effect", shifting the Dirac point to lower gate voltages (**Figure 2c**) [25]. This is due to the potential drop over the electrical double layer (EDL) in solution – increasing the ionic strength, decreasing the Debye length, which in turn increases the double layer capacitance and reduces the surface potential for a given surface charge. On the other hand, lowering the ionic strength will reduce the doping, shifting the Dirac point towards more positive values [26]. Moreover, using ionic strength buffer below 0.01× has a negative effect, since the low ion concentration present no longer induces a gating effect, preventing proper transistor's performance. Ten times higher ionic strength (0.01× PBS) enables the gating of the

device, visible by a large increase on device's V-shape. Importantly, to discard the hypothesis that the change of the Dirac point could be due to drift over time, we recorded several transfer characteristics of our devices in 0.01× PBS and observed no significant shift of the curves (Data not shown). The leakage current is also shown and demonstrated to be several orders of magnitude smaller than the electronic response signal (**Figure S4**), being considered neglectable.

Knowing that field-effect transistors performing in a liquid environment are highly dependent on the electrolyte ions as well as analyte charges, careful choice and analysis of the working medium should be considered. To understand better the gating effect in biological fluids, the transfer characteristics of the aptamer:PEG modified graphene channel were in addition assessed in more complex bodily fluids: serum, saliva, sweat and exhaled breath condensate (EBC) (**Figures 3a-d**). Having the 1x PBS curve as a reference in all plots, which results in a Debye length of approximately 0.72 nm, we can make a correlation and predict that undiluted serum and saliva are more concentrated than PBS, and we can estimate that the Debye length might be even shorter – worsening the ion screening effect, thus making biosensing in these fluids with the gFET quite complex and though to overcome. On the other hand, analysing the curves from sweat we can stipulate that the behaviour will be relatable to that of PBS. In the case of EBC, these fluids are believed to contain less ions than serum, saliva and sweat, which agrees with the Dirac point values observed – the Dirac point remains positive in EBC samples even at high concentrations. In fact, EBC contains nearly 3500 components which mainly include volatile organic components, oxidation by-products (hydrogen peroxide, isoprostanes, nitrates and nitrites, etc) and eventual biomarkers [27, 28], making this a promising biological fluid to work with gFETs. Also, on this case, the leakage current for each media is shown and demonstrated to be several orders of magnitude smaller than the electronic response signal (**Figure S5**), being considered neglectable.

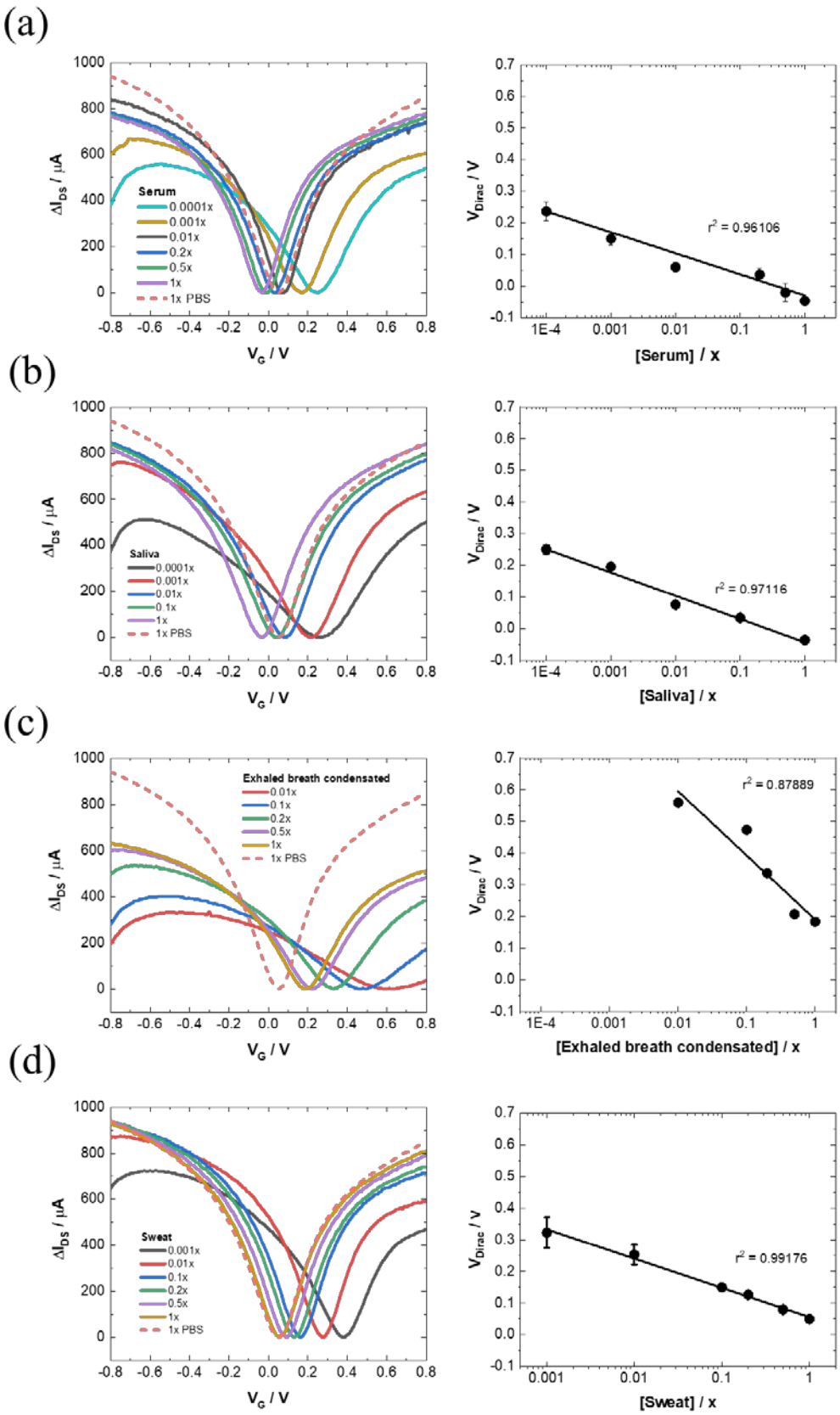

Figure 3: Aptamer:PEG-gFET characteristics in serum, saliva, sweat and exhaled breath condensate (EBC). (a) Transfer characteristics of different concentrations of bodily fluids diluted in water, together with the change of Dirac point in (a) serum, (b) saliva, (c) EBC and

(d) sweat samples. n=3. The current values were treated to start at zero using the equation ΔI_{DS} = I_{DS}-minimum(I_{DS}). See Figures S5 for raw data and gate leakage current values.

Electrical response to cardiac troponin I in 0.01× PBS

The PEG:aptamer modified GFET was further investigated for its ability to convert the binding interaction with different cTnI concentrations into an electrical signal. The transfer characteristics of the modified-graphene FET during exposure to cTnI solutions from 3 to 1000 pg mL^{-1} in 0.01× PBS were recorded after 10 min stabilization for each concentration (**Figure 4a**). No change in the shape of the $I_{DS}V_{GS}$ curves were observed besides a cathodic shift in the Dirac point (**Figure 4b**) and a positive and a negative shift of the I_{DS} in the electron and hole regimes, respectively.

Figure 4c shows clearly a cTnI dependent increase in the FET source-drain current in the holes' regime (fixed V_G = 350 mV). This comes as a consequence of the positively charged molecules adsorbed onto the channel: since cTnI has an isoelectric point of 9.87, it is positively charged at physiological pH. This induces a negative charge in the graphene channel, generating more electrons, making them the majority carriers. The $I_{DS}V_{GS}$ curve shifts to the left side due to graphene's n-doping, leading to a decrease of the Dirac Point. This suggests that the decrease of the Dirac point value is attributed to the charge gating effect of the attached linker molecules and cTnI. The exact opposite is observed in the electrons' regime (fixed V_G = 200 mV (**Figure 4d**)). By performing a linear fit to the measurement data in the linear regime (3 - 60 pg mL^{-1}), the sensitivity of the FET, defined as $\Delta I_{DS}/\Delta C_{cTnI}$, was determined to be 1.09734 µA/pg mL^{-1}. This sensitivity, along with the estimated noise level of 1.2207 µA for the measurement system, was used to determine the limit of detection (LoD) defined as: LoD = (S/N × Noise)/Sensitivity. The recorded LoD was found to be equal to 3.34 pg mL^{-1} (S/N = 3), way below the threshold for diagnostically relevant levels of cardiac troponin I (25 pg mL^{-1}). Moreover, the dynamic response of the GFET covers the concentrations range relevant for patient diagnostic with cTnI critical levels (25 pg mL^{-1} – 50 pg mL^{-1}).

Using the Langmuir isotherm format on equation (3), and assuming a 1:1 complex between the antigen (cTnI) from solution and the aptamer receptor on the sensor surface, the affinity constant K_A can be determined by plotting the surface coverage Θ - the I_{DS} at a given cTnI concentration, $I_{DS}(c_0)$, divided by the $I_{DS}(c_\infty)$, the drain-source current at infinite bulk analyte concentration.

$$\boldsymbol{\Theta} = \frac{\boldsymbol{I_{DS}(C_0)}}{\boldsymbol{I_{DS}(C_\infty)}} = \frac{\boldsymbol{K_A \times C_0}}{\boldsymbol{1 + K_A \times C_0}} \qquad (3)$$

A dissociation constant (i.e., a half saturation-constant) K_D = 51.4 pg mL^{-1} for the electrons' regime and K_D = 53.2 pg mL^{-1} for the holes' regime were calculated by fitting the data. Moreover, our GFETs can be analyzed on both regimes of the $I_{DS}V_{GS}$ curves, where K_D values of the same order can be obtained from both analyses, indicating not only a good symmetry of our devices, but also good stability.

In the end, the aptamer used proved to be selective for cTnI **(Figure 4e-f**), whereas using a scrambled aptamer for cTnI detection resulted in much smaller current responses with increased cTnI concentrations. This confirms the specificity of our sensing device towards cTnI, which is again confirmed when recording the current changes using another cardiac troponin protein, BNP-32 (**Figure 4f**). Although having almost identical isoelectric point (from 9 to 10), a decrease in current was observed. As pointed out by Nakatsuka et al., [29] charge is not the only element dictating FET behaviour, and different conformation changes upon target binding are proposed, where a current decrease is consistent with aptamer reorientation towards the sensing channel. More specifically, the increase of negatively charged backbones is depleting channels electrostatically (case of BNP), while aptamer stem-loops reorientation away from the graphene channel increases transconductance as in the case of cTnI.

The reproducibility of the electrode fabrication was determined on 9 devices (**Figure S6**), and the long-term stability of the sensor showed a loss of 4% when tested in cTnI (100 pg mL^{-1}) upon storage of the electrode at 4◦C for a month. The sensor can be regenerated by immersion into NaOH (0.1 M, pH 12.0) for 20 min.

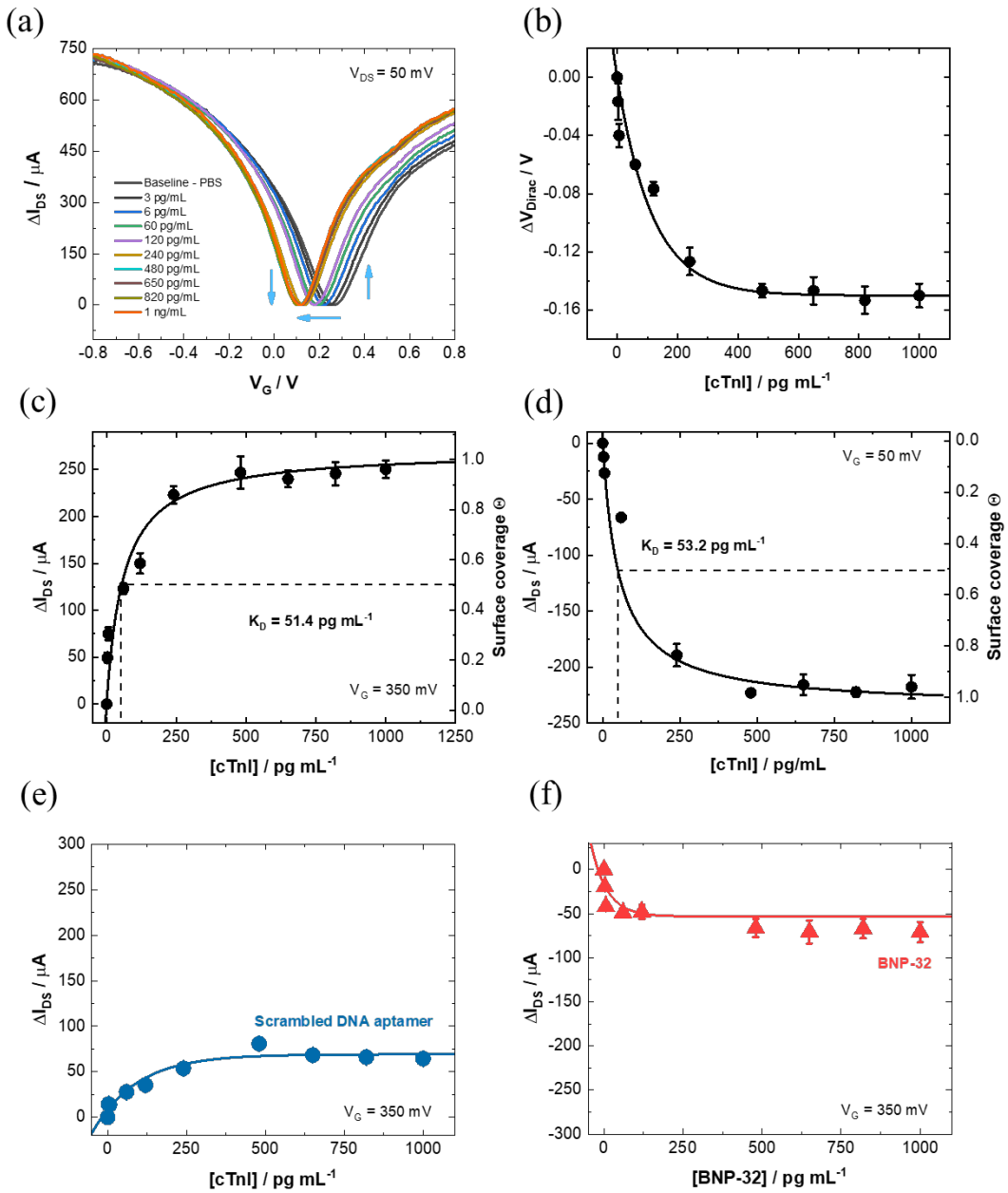

Figure 4: GFET based sensing of cTnI in 0.01 x PBS. (a) Graphene transfer characteristics after stabilization for each cTnI concentration (3, 6, 60, 120, 240, 480, 650, 820 and 1000 pg mL^{-1}) in 0.01× PBS (pH 7.4) without washing steps, with applied V_{DS} = 50 mV. (b) Change of Dirac Point for each concentration. (c) ΔI_{DS} for each cTnI concentration at a fixed gate voltage V_G = 350 mV with respective Langmuir binding isotherm. (d) ΔI_{DS} for each cTnI concentration at a fixed gate voltage V_G = 200 mV with respective Langmuir binding isotherm. (e) ΔI_{DS} for each cTnI concentration interacting with a scrambled aptamer at a fixed gate voltage V_G = 350 mV. (f) ΔI_{DS} for each BNP-32 concentration interacting with cTnI aptamer at a fixed gate voltage V_G = 350 mV. n=3. The current values were treated to start at zero using the equation ΔI_{DS} = I_{DS}-minimum(I_{DS}). See Figure S7 for raw data and gate leakage current values.

Cardiac troponin I detection in spiked human serum

As device's response is highly dependent on the ionic strength of the solution, we pushed the study further and investigated the electrical current I_{DS} of the aptamer:PEG-modified GFETs upon exposure to 240 pg mL^{-1} of cTnI in PBS at different concentrations (**Figure 5a,** raw data see **Figures S8**). As expected, the current change is less prominent while increasing the solution's ionic strength with signals detectable at 0.1× PBS. When plotting the change in electrical current, ΔI_{DS}, upon exposure to 240 pg mL^{-1} of cTnI in PBS at different concentrations on PEG-, aptamer-, and PEG:aptamer-modified GFETs, only the PEG:aptamer sensor displayed a linear relation of ΔI_{DS} with PBS concentration and allowed the detection of cTnI at 0.1× PBS **(Figure 5b**). We thus demonstrate that the presence of PEG units in the sensing layer is not only essential to diminish anti-fouling effects, but also increases the effective screening length due to ion buffering [4].

To achieve protein concentration-dependent sensing, we opted for investigating the possibility of using two-different desalination columns for pre-treatment: Zeba™ Spin Desalting Columns (column A) based on centrifugation and the Sephadex® (crosslinked dextran gel) G-25 packed one (column B) using gravity for separation. Both columns, in particular column B, resulted in $I_{DS}V_{GS}$ curves comparable to 0.01× PBS (see SI, **Figure S8b**). To evaluate the feasibility of this approach, human serum spiked with 100 pg mL^{-1} cTnI was passed through both columns and the amount of cTnI in the desalinated solution was determined (**Table 1**) using a calibration curve generated using ELISA (**Figure S8a**).

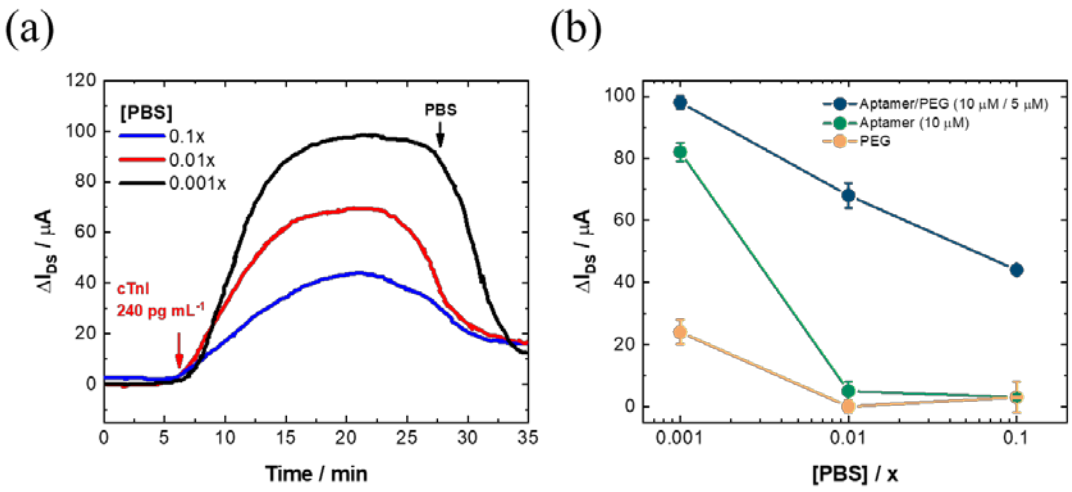

Figure 5: GFET based sensing of cTnI in PBS of different concentrations. (a) Time dependent measurements of 240 pg mL^{-1} cTnI in 0.001× PBS (black), 0.01× PBS (red) and 0.1× PBS

(blue) with regeneration after buffer washing. V_G = 350 mV. The current values were treated to start at zero using the equation ΔI_{DS} = I_{DS}-StartingPoint(I_{DS}). See **Figure S8** for raw data. (b) I_{DS} shift for 240 pg mL^{-1} cTnI in 0.001× PBS, 0.01× PBS and 0.1× PBS using a GFET surface modified with aptamer:PEG 2:1 mixture (blue), aptamer only (grey) and PEG only (black).

Table 1: cTnI concentrations determined from the calibration curve presented in Figure S9.

sample	Optical density	cTnI [pg mL^{-1}] ELISA	cTnI [pg mL^{-1}] GFET
HS	0.112	nd	nd
HS[1]+100 pg mL^{-1} cTnI	0.221	85 ± 15	95 ± 3
HS+100 pg mL^{-1} cTnI passed via Colume A[2]	-	nd	nd
HS+100 pg mL^{-1} cTnI passed via Colume B[3]	0.133	51 ± 6	54 ± 4

[1]HA=human serum; [2]column A: Zeba™ Spin Desalting Column (Thermofisher)
[3]column B: PD 10 Desalting Column (Cytiva); nd=not detectable

As shown in Table 1, column A resulted not only in desalination, but also in capture and/or degradation of cTnI. Column B on the other hand, led to desalination and dilution of the cTnI by half. Out of the 100 pg mL^{-1} added to human serum, 51 pg mL^{-1} were recovered according to ELISA measurements – this is in agreement with the column specifications. This measurement is in addition on the sensitivity limit of the ELISA sensor (**Figure S9**), being about 48 pg mL^{-1} cTnI. Furthermore, measurement of these samples on the aptamer-modified GFET (**Figure 5c**) agrees with the value given by ELISA and using the cTnI calibration curve generated in 0.01× PBS (**Figure 4c**), a cTnI concentration of 54 ± 4 pg mL^{-1} was determined, once again, in agreement with ELISA results (**Table 1**). Indeed, interaction with BNP gives a small positive shift of the $I_{DS}V_{GS}$ curve (**Figure 5d**), indicative of non-specific interaction.

Evaluation on clinical samples

To further evaluate the applicability of the developed point of care device for troponin I sensing in serum, patient samples, provided by CHU Lille from the ongoing clinical POMI-AF study (Principal investigator David Montaigne; Clinical trial # NCT03376165), were investigated with the GFET sensor. Patients were included after informed consent before undergoing cardiac surgery and blood samples were obtained the days following surgery to monitor peri-operative cardiac injury. Samples of 15 patients with different troponin levels were analysed (**Table 2**) for their troponin T and troponin I levels. The 15 patients were grouped according to the magnitude of peri-operative myocardial injury as assessed by clinical hs-cTnT assay (measured

using Elecsys Troponine T-hs, Roche Diagnostics, Meylan, France), i.e. mild (cTnT <15 pg mL^{-1}), moderate (15 pg mL^{-1}> c-TnT <500 mL^{-1}), severe (cTnT >500 pg/mL), and corresponding to 3 troponin zones (respectively, low, medium and high) [30]. 400 µL of each sample was measured on the GFET device and the transfer characteristics were determined. The transfer characteristics during exposure to a patient sample from each troponin zone (low-medium-high) was recorded after 10 min stabilization for each sample (**Figure 6a**). Cathodic shifts of the Dirac points are observed (**Figure 6b**) when measuring low-medium-high troponin patient samples as expected with a positive and a negative shift of the I_{DS} in the electron and hole regimes, respectively (**Figure 6c**), in agreement with Figure 4. From the ΔI_{DS} values determined for each sample and using the calibration curve of Figure 4c, cTnI concentrations were extracted (**Table 2**), in which low and medium cTnI levels in the patient samples were clearly distinguished. For high cTnI levels, the sensor was in its saturated state and one could only say that concentrations >500 pg mL^{-1} are present in the sample. Interestingly, the GFET sensor allowed sensing the very low cTnI levels, where the use of the ELISA kit was not sensitive to anymore. With a limit of detection of 3.34 pg mL^{-1} (S/N = 3) in 0.01× PBS, the sensor has an adapted sensitivity to distinguish healthy patients with increased cTnI levels. While indeed a larger patient sample collection is required for clinical assessments, these data seem highly promising.

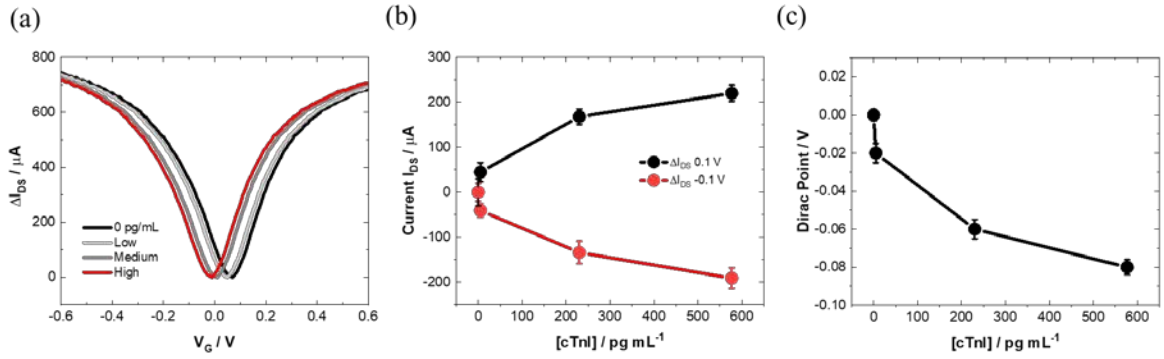

Figure 6: (a) CTnI aptamer modified GFET transfer characteristics for each patient sample: low-medium-high troponin concentration corresponding to the classification according to **Table 2**. (b) Change of I_{DS} of patient samples of low-medium-high troponin levels (V=0.1 and -0.1 V). (c) Change of Dirac point of patient samples of low-medium-high troponin levels. n=3. See **Figures S10** for raw data and gate leakage current values.

Table 2: Analysis of 15 patient samples via ELISA and aptamer-modified GFET measurements: 3 groups are identified: low levels of troponin (bright grey zone), elevated troponin levels (dark grey zone) and high levels (red zone).

Patient	cTnT (pg/mL) ELISA	cTnI [pg mL^{-1}] ELISA	ΔI_{DS} [µA]	cTnI [pg mL^{-1}] GFET
2	13171	6258	275	>500
1	1398	610	275	>500
4	671	225	245	250
3	577	195	225	200
6	272	110	193	111
5	254	102	190	107
8	250	100	185	98
10	230	92	183	97
9	222	88	175	70
11	10	5	45	5±1
12	5	nd	35	4±1
13	5	nd	35	4±1
14	5	nd	45	5±1
15	6	nd	45	5±1

nd=not detectable

Conclusion

The gold standard diagnostic tool of acute myocardial infarction (AMI) in clinical settings remains ELISA-based assay. In this work, we propose a graphene-based field effect transistor as a high-sensitive point-of-care cTnI testing assay. The proposed electrical sensor achieved cTnI detection at a ten-fold lower concentration than the 40 pg mL^{-1} cut-off for detecting myocardial injury and allowed to differentiate healthy patients from patients with myocardial ischemia in less than 10 minutes. With a limit of detection of 3.34 pg mL^{-1} (S/N = 3) in 0.01× PBS, the sensor has an adapted threshold for diagnosis of relevant levels of cardiac troponin I. CTnI was also quantified in spiked human serum samples via the pre-treatment of the solution using a disposable desalting column packed with Sephadex, a cross-linked dextran gel. Gravitation filtering of 2.5 mL of cTnI spiked human serum sample resulted in a solution of ionic strength comparable to 0.01× PBS, adapted for the developed sensor. While this approach resulted in a 50% dilution of cTnI, the protein could still be detected using our GFETs.

The question might be raised if it is likely that an assay, such as the one described here, that can detect troponin levels below the reference range, will produce clinical benefits. In our mind, quantifying cardiac troponin in blood samples from patients with very low, and presently

undetectable levels, will allow to refine cardiovascular risk stratification in patients with cardiovascular risk factors such as tobacco use, type 2 diabetes, dyslipidaemia and obesity, even in the absence of cardiovascular medical history or symptoms. This would thus, improve the tailoring of preventive measures and medication in a personalized manner. Moreover, we strongly believe that the implementation of fast and sensitive cTnI point-of-care sensors in emergency departments will be beneficial for patients. Not to mention, the approach used in this work is easily applicable to the sensing of other biomarkers in biological matrixes of high ionic strength.

Acknowledgement

Financial support from the Centre National de la Recherche Scientifique (CNRS), the University of Lille, CPER "Photonics for Society" and I-Site is acknowledged. DM, LB and EW are supported by grants from Agence Nationale pour la Recherche (ANR-10-LABX-0046, ANR TOMIS-Leukocyte: ANR-CE14-0003-01 and ANR CALMOS: ANR-18-CE17-0003-02), the Leducq Foundation LEAN Network 16CVD01 and the National Center for Precision Diabetic Medicine–PreciDIAB (ANR-18-IBHU-0001; 20001891/NP0025517; 2019_ESR_11).

Experimental Section

Materials: Phosphate buffer tablets (PBS, 0.1 M), tetrabutylammonium fluoride (TBAF), copper(II) sulfate ($CuSO_4$), L-ascorbic acid, ethylenediaminetetraacetic acid (EDTA), N-butyl hexafluorophosphate (NBu_4PF_6), methoxypolyethylene glycol azide PEG (average Mn=2,000), and ferrocenemethanol were purchased from Sigma-Aldrich and used as received. Azidomethylferrocene was synthesized according to Reference [31]. 4-((trisopropylsilyl)ethylenyl)benzenediazonium tetrafluoroborate (TIPS-Eth-ArN_2^+) was synthesized as reported previously [32]. The 5'-azide modified troponin I aptamer (5'-N_3-TTT-TTT-CGT GCA GTA CGC CAA CCT TTC TCA TGC GCT GCC CCT CTT A-3') was purchased from integrated DNA Technologies (Leuven, Belgium). The unspecific aptamer was

a 5'-azide modified Brain Natriuretic Peptide-32 aptamer (5′-N_3-TTT-TTT-GGC GAT TCG TGA TCT CTGCTC TCG GTT TCG CGT TCG TTC G-3′).
Graphene is synthesized in-house as described below. Interdigitated microelectrodes (ED-IDE1-Au w/o SU8) are provided by Micrux Technologies.
Zeba™ Spin Desalting Columns, 7K MWCO, 2 mL (ref. 89890) (Column A in this work) were purchased from Thermofisher, France. Disposable PD 10 Desalting Columns (ref. 17-0851-01, column B in this work) were purchased from Cytiva, France.
Human Cardiac Troponin I ELISA Kit (ref. ab200016) was purchased from ABCAM.
Recombinant human cardiac troponin I protein (MW=24 kDa) was obtained from Abcam (Cambridge, UK). NP-32 peptide (MW = 3.4 kDa) was obtained from BACHEM AG (Switzerland).

Human serum samples were provided by CHU Lille from the ongoing clinical POMI-AF study (Principal investigator David Montaigne; Clinical trial # NCT03376165), approved by the local Ethics Committee. Patients were included after informed consent before undergoing cardiac surgery and blood samples were obtained one day following surgery to monitor peri-operative cardiac injury.
For each patient, 4 mL of venous blood were collected on EDTA-tubes (BD vacutainer), centrifugated and immediately aliquoted in 500 µL for storage (-80°C).
The magnitude of peri-operative myocardial injury was assessed in the peri-opeartive period thanks to the clinical hs-cTnT assay Elecsys Troponine T-hs, Roche Diagnostics (Meylan, France) and was grouped in mild (c-TnT <15 pg/mL), moderate or severe (>500 pg/mL) myocardial injury, corresponding to 3 troponin zones (respectively, low, medium and high).[30]

Graphene synthesis: The monolayer graphene is grown by chemical vapor deposition (CVD) on commercial Cu foil from Alpha Aesar (high purity - 99.9999%). Graphene growth is carried out in a Jipelec JetFirst Rapid Thermal CVD (RTCVD). This system allows heating and cooling at high rates (10 °C s^{-1}). The growth itself comprises heating, annealing, growth and cooling steps. We used a mixture of 100 sccm of argon and 5 sccm of dihydrogen during all the steps and 20 sccm of methane as a precursor during the growth phase. We first cut the Cu foil in small pieces (2.5 × 2.5 cm), clean them with acetic acid, acetone and IPA for 5 min each under ultrasonication in order to remove all possible copper oxide and to produce the cleanest surface possible. We then put the pieces onto a Si wafer in the chamber. We proceed to a high vacuum

(< 5×10^{-5} bar) before starting and then the sample is heated for 5 min from room temperature to 300 °C, followed by 2 min from 300 °C to 1070 °C, annealing for 5 min, growth for 5 min and finally a quick cooling of the chamber using a water flow (with a decrease rate of 60 °C s^{-1} from 1000 to 700 °C), for 10 min to reach room temperature.

FET sensor fabrication: Prior to graphene transfer, the interdigitated microelectrodes (ED-IDE1-Au w/o SU8, Micrux Technologies) are cleaned in an UV-Ozone chamber (Jelight, USA) for 10 min followed by submersion for 15 min sequentially in 10 mL of acetone, isopropanol and water. Finally, every chip is copiously rinsed with large amount of water and dried under a nitrogen flow. The cleaned interfaces are placed in a plastic Petri dish and stored in a desiccator under vacuum. The cleaned IDE are modified with trimethoxyphenylsilane (TMPS, 300 µL of TMPS in 15 mL of ethanol) in a plastic falcon tube for 1 h. Afterwards, the electrodes are immersed for 15 min in ethanol to remove the excess of the silane compound from the surface. Subsequently, the modified interfaces are nitrogen blow-dried and stored under vacuum. The chips are placed on a hot plate at 120 °C at ambient pressure for 1 h to anneal the formed monolayer and provide complete removal of the solvents from the surface. Graphene is directly transferred to these interfaces. For graphene transfer, a polymethyl methacrylate (PMMA) film of 200 nm in thickness is spin-coated onto the graphene/Cu foil and annealed at 110 °C with a very slow heating and cooling rate (1 °C min^{-1}) in order to prevent cracks in the graphene due to the difference of the thermal expansion coefficient between copper and graphene. The graphene on the back side of the Cu foil was removed by reactive ion etching (RIE) in an O_2 plasma (50 W/100 mT/25 sccm/1 min). Copper foil etching was achieved in 0.2 M ammonium persulfate ($(NH_4)_2S_2O_8$) for 8 h and the floating PMMA/graphene sample was put in a DI water. This operation was repeated about 10 times in order to rinse the graphene from the etchant solution. Graphene transfer onto the IDE was achieved by submerging the IDE under the floating graphene/PMMA film. To remove traces of trapped water between graphene and IDE and to increase the adhesion of graphene to the IDE, the substrate was placed on a hot plate and annealed at 90 °C for 30 min using a slow heating and cooling rate (1 °C min^{-1}). The PMMA layer was effectively removed by UV/ozone cleaning (28-35 mW cm^{-2}) for 5 min followed by a hot acetone rinse (30 °C for 30 min).

Surface modification: The electrografting of 4-((trisopropylsilyl)ethylenyl)benzenediazonium tetrafluoroborate (TIPS-Eth-ArN_2^+) (10 mM) in 0.1 M N-butyl hexafluorophosphate (NBu_4PF_6) in acetonitrile was performed using cyclic voltammetry at a scan rate of 50 mV s^{-1} for five cycles between +0.20 V and -0.60 V vs. Ag/AgCl. The electrodes were rinsed with copious

amounts of acetonitrile and acetone, and gently dried. Before "click" chemistry, the TIPS protection group was removed by immersion of the graphene-TIPS surface into tetrabutylammonium fluoride (TBAF, 0.1 M in THF) for 1h at room temperature. The surface was then left for 15 min in a pure THF solution for cleaning. This modification process produces an ethynyl-terminated GFET. The deprotected surface was then exposed to polyethylene glycol (mPEG-N_3, Mn 2000) and azide-DNA aptamer mixture (5 µM:10 µM or 20 µM:10 µM) in a ratio of 1:2 pr 2:1 using $CuSO_4$ (0.01 M) and L-ascorbic acid as reaction catalyst. The interface was then treated with an aqueous solution of EDTA (10 mM) for 10 min to chelate any remaining Cu^{2+} residues and finally washed copiously with water and left to dry.

Electrical sensing: Electrical measurements were conducted using a probe station source meter unit U2322A (Keysight Technologies, USA). All measurements were performed using a PMMA commercial flow cell (Micrux Technologies, Spain) with fixed flow channel geometry (16 µL), ensuring a defined flow rate of 50 µL min^{-1} to minimize mass transport limitation of the analyte to the sensor surface in all experiments. A silver chloride wire (diameter 1 mm, Sigma-Aldrich) was used to operate the GFET device in liquid gate configuration, with a constant gate bias (V_{GS}) of -0.1 V and a constant source-drain bias (V_{DS}) of 0.05 V, sweeping the gate voltage (VG) between -0.8 V and +0.8 V. Choosing 0.05 V as V_{DS} bias results in high current outputs due to the high conductivity of graphene; however, this value is still inserted in the linear regime of the output curves (**Figure S11**). The general procedure of the sensing experiment started with continuously flushing the pure buffer (PBS, 0.01×) until a stable baseline of drain current was established, followed by injection of the analyte at a constant flow rate of 50 µL min^{-1}.

Desalination method: 2.5 mL of the human serum sample with cTnI were added to one of the desalination columns and passed through the column using 3.5 mL of 0.01× PBS. 50 µL of this solution was then used for ELISA analysis and the rest for GFET sensing.

Characterization: Scanning electron microscopy (SEM) images were obtained using an electron microscope ULTRA 55 (Zeiss, France) equipped with a thermal field emission emitter and three different detectors (EsB detector with filter grid, high efficiency In-lens SE detector and Everhart-Thornley Secondary Electron Detector). Raman spectroscopy measurements were performed on a LabRam HR Micro-Raman system (Horiba Jobin Yvon, France) combined with a 473 nm laser diode as excitation source. Visible light was focused by a 100× objective. The

scattered light was collected by the same objective in backscattering configuration, dispersed by an 1800 mm focal length monochromator and detected by a CCD. Electrochemical measurements were performed on a potentiostat/galvanostat/impedance analyzer (PalmSens4, PalmSens, The Netherlands). A conventional three-electrode configuration was employed using a silver wire and a platinum mesh as the reference and auxiliary electrodes, respectively.

References

[1] E. Giannitsis, V. Gopi, Herz 45 (2020) 509–519.
[2] P.A. Kavsak, J. MacCuish, J. Boreyko, C. Roy, S. Lamers, L. Clark, Clin. Biochem., 69 (2019) 52-56.
[3] R.H. Christenson, W.F. Peacock, F.S. Apple, A.T. Limkakeng, R.M. Nowak, J. McCord, C.R. deFilippig, Contemp. Clin. Trials Commun. , 14 (2019) 100337.
[4] N. Gao, T. Gao, X. Yang, X. Dai, W. Zhou, A. Zhang, C.M. Lieber, PNAS, 51 (2016) 14633-14638.
[5] Y. Ohno, K. Maehashi, K. Matsumoto, J. Am. Soc. , 132 (2010) 18012-18013.
[6] X. Dong, Y. Shi, W. Huang, P. Chen, L.-J. Li, e. al, Adv. Mater., 22 (2010) 1649-1653.
[7] W. Fu, L. Jiang, E.P. van Geest, L.M.C. Lima, G.F. Scheider, Adv. Mater., 29 (2016) 1603610.
[8] N. Kumar, M. Gray, J.C. Ortiz-Marquez, A. Weber, C.R. Demond, A. Argun, T. can Opijnen, K.S. Burch, Med. Devices Sens., 3 (2020) e10121.
[9] F. Schwierz, Nat. Nanotechnol., 5 (2010) 487–496.
[10] C. Reiner-Rozman, C. Kotlowski, W. Knoll, Biosensors, 6 (2016) 17.
[11] C. Reiner-Rozman, M. Larisika, C. Nowak, W. Knoll, Biosens. Bioelectron., 70 (2015) 21–27
[12] C.-J. Shih, Q.H. Wang, Z. Jin, G.L.C. Paulus, D. Blankschtein, P. Jarillo-Herrero, M.S. Strano, Nano Lett., 13 (2013) 809-817.
[13] A. Sinitskii, A. Dimiev, D.A. Corley, A.A. fursina, D.V. Kosynjin, J.M. Your, ACS Nano, 4 (2010) 1949-1954.
[14] G.L.C. Paulus, Q.H. Wang, S.M. E., Acc. Chem. Res., 46 (2012) 160-170.
[15] V. Mishyn, T. Rodrigues, L.Y. R., P. Aspermair, H. Happy, J. Bintinger, C. Kleber, R. Boukherroub, W. Knoll, S. Szunerits, Nanoscale Horiz., 6 (2021) 819-829.
[16] T. Rodrigues, V. Mishyn, A. Bozdogan, Y.R. Leroux, H. Happy, A. Kasry, R. Boukherroub, J. Dostalek, P. Aspermair, J. Bintinger, C. Kleber, S. Szunerits, W. Knoll, Ann. Clin. Med. Case Rep., 6 (2021) 1-16.
[17] F. Chekin, V. Vasilescu, R. Jijie, S.K. Singh, S. Kurungot, M. Iancu, G. Badea, R. Boukherroub, S. Szunerits, Sensors and Actuators B: Chemical, 261 (2018) 180-187.
[18] W. Gwei, X. Zhou, G. Deokar, H. Kim, M.M. Belhaj, E. GAloin, E. Pallecchi, D. Vignaud, H. Happy, IEEE Trans. Electron Devices 9(2015) 2769-2773
[19] Z. Xia, F. Leonardi, M. Gobbi, Y. Liu, V. Bellani, A. Liscio, A. Kovtun, R. Li, X. Feng, E. Origu, P. Samori, E. Treossi, V. Palermo, ACS Nano, 10 (2016) 7125-7134.
[20] J. Park, M. Yan, Acc. Chem. Res., 46 (2012) 181-189.
[21] C.E.D. Chidsey, C.R. Bertozzi, T.M. Putvinski, A.M. Mujsce, J. Am. Chem. Soc., 112 (190) 4301−4306.
[22] N.C.S. Vieira, J. Borme, G.J. Machado, F. Cerqueira, P.P. Freitas, V. Zucolotto, N.M.R. Peres, P. Alpumin, J. Phys.: Condens. Matter, 28 (2016) 085302.

[23] I. Alam, K. Sa, S. Das, B.V.R.S. Subramanyam, S. Subudhi, M. Mandal, S. Patra, B. Samanta, R.R. Sahu, S. Swain, A. Mahapatra, P. Kumar, P. Mahanandia, Solide Stat Commun., 340 (2021) 114533.
[24] A. Svetlova, D. Kireev, G. Beltramo, D. Mayer, A. Offenhäusser, ACS Appl. Electron. Mater., https://doi.org/10.1021/acsaelm.1c00854 (2021).
[25] J. Ping, J. Xi, J.G. Saven, R. Liu, A.T.C. Johnson, Biosens. Bioelectron., 89 (2017) 689-692.
[26] I. Heller, S. Chatoor, J. Männik, M.A.G. Zevenbergen, C. Dekker, S.G. Lemay, J. Am. Chem. Soc., 132 (2010) 48.
[27] J. Hunt, Immunol. Allergy Clin. North. Am. , 27 (2007) 587.
[28] S. Dodig, I. Čepelak, Biochem Med, 23 (2013) 281–295.
[29] N. Nakatsuka, K.-A. Yang, J.M. Abendroth, K.M. Cheung, X. Xu, H. Yan, C. Zhao, B. Zhu, Y.S. Rim, Y. Yang, P.S. Weiss, M.N. Stonjanovic, A.M. Andrews, Science, 362 (2018) 319-324.
[30] D. Montaigne, X. Marechal, T. Modine, A. Coisne, S. Mouton, G. Fayad, S. Ninni, C. Klein, S. Ortmans, C. Seunes, C. Potelle, A. Berthier, C. Gheeraert, C. Piveteau, R. Deprez, J. Eeckhoute, H. Duez, D. Lacroix, B. Deprez, B. Jegou, M. Koussa, J. Edme, P. Lefebvre, B. Staels, Lancet, 391 (2018) 59-69. .
[31] J.M. Casas-Solva, A. Vargas-Berenguel, L.F. Captian-Vallvey, F. Santoyo-Gonzalez, Org. Lett. , 6 (2004) 3687–3690.
[32] Y.R. Leroux, P. Hapiot, Chem. Mater., 25 (2013) 489-495.

SUPPORTING INFORMATION

Highly performing graphene-based field effect transistors for the label-free electrical detection of cardiac troponin I in serum

Teresa Rodrigues,[1,2] Vladyslav Mishyn,[1,2] Yann R. Leroux,[3] Laura Butruille,[4] Eloise Woitrain,[4] Alexandre Barras,[1] Patrik Aspermair,[2] Henri Happy,[1] Christoph Kleber,[5] Rabah Boukherroub,[1] David Montaigne,[4] Wolfgang Knoll,[5]* and Sabine Szunerits[1*]

[1] *Univ. Lille, CNRS, Centrale Lille, Univ. Polytechnique Hauts-de-France, UMR 8520 - IEMN, F-59000 Lille, France*

[2] *AIT Austrian Institute of Technology GmbH, Biosensor Technologies, 3430 Tulln, Austria*

[3] *Univ. Rennes, CNRS, ISCR – UMR 6226, Campus de Beaulieu, F-35000 Rennes, France*

[4] *Univ. Lille, Inserm, CHU Lille, Institut Pasteur de Lille, U1011- EGID, F-59000 Lille, France*

[5] *Department of Physics and Chemistry of Materials, Faculty of Medicine/Dental Medicine, Danube Private University, Krems, Austria*

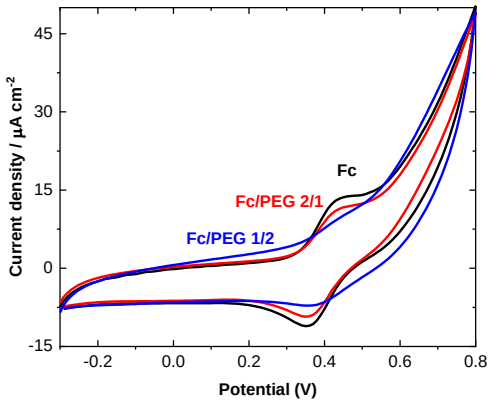

Figure S1: Determination of the surface coverage upon clicking azide-ferrocene and azide-PEG units to the ethynyl-terminated GFET. Linear sweep voltammograms of the interface in

* To whom Correspondence should be send to: wolfgang.knoll@ait.ac.at, sabine.szunerits@univ-lille.fr

acetonitrile/NBu_4FP_6 (0.1 M), scan rate=100 mV s^{-1}. The surface coverage was determined from the integration of the cyclic voltammogram using equation (1):

$$\Gamma = Q/nFA \quad (1)$$

where Q is the passed charge (C), n the number of exchanged electrons (n=1), F the Faraday constant (96.485 C mol^{-1}) and A is the electroactive surface of the electrode determined as 0.1 cm^2.

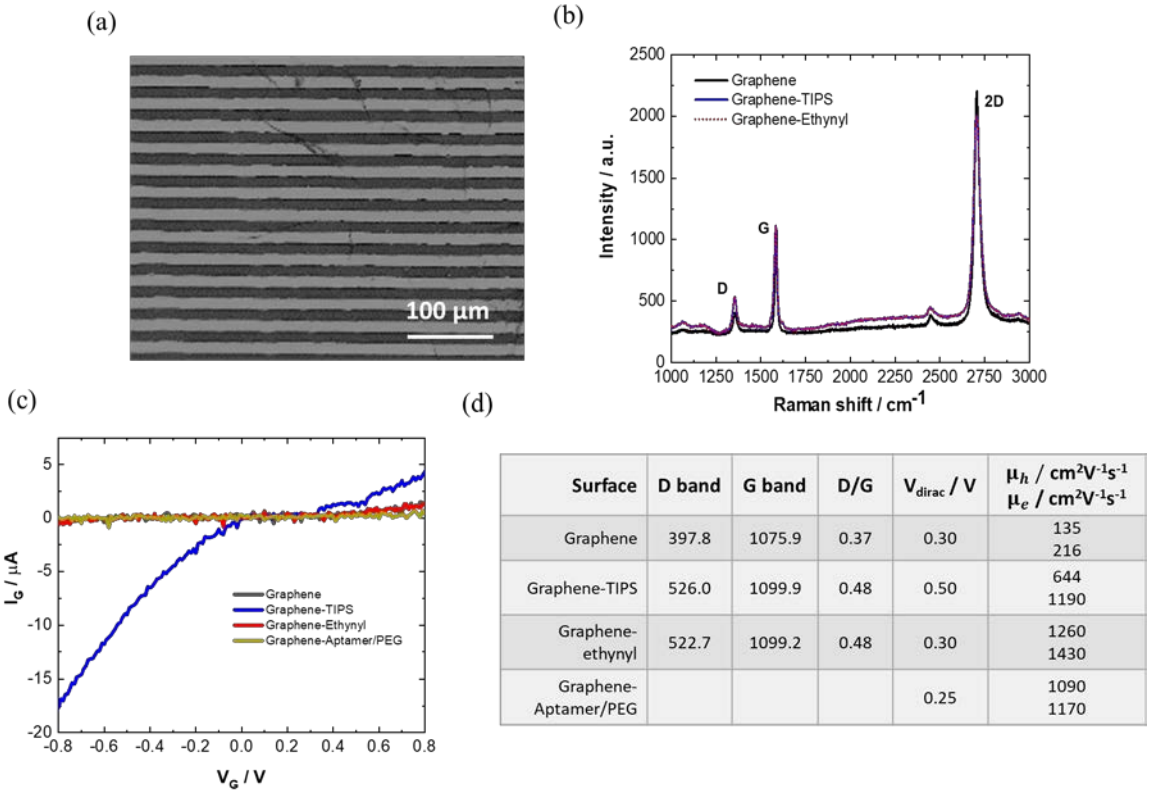

Surface	D band	G band	D/G	V_{dirac} / V	μ_h / $cm^2V^{-1}s^{-1}$ μ_e / $cm^2V^{-1}s^{-1}$
Graphene	397.8	1075.9	0.37	0.30	135 216
Graphene-TIPS	526.0	1099.9	0.48	0.50	644 1190
Graphene-ethynyl	522.7	1099.2	0.48	0.30	1260 1430
Graphene-Aptamer/PEG				0.25	1090 1170

Figure S2: Characterisation of GFET sensor. (a) SEM image of CVD graphene coated IDE. (b) Raman spectra of graphene before and after transfer and chemical modification with aptamer/PEG units. (c) Leakage current (leakage at the gate electrode) taken from an unmodified GFET (grey), after diazonium grafting (blue), after TIPS deprotection (red) and after aptamer/PEG immobilization (yellow). (d) Table of mobility carriers and Raman data for the four different interfaces determined in 0.01× PBS.

The anodic hole mobility, μ_h, and cathodic electron mobility, μ_e, were obtained from the anodic and cathodic linear slopes of the $I_{DS}V_{GS}$ plots using equation μ_e or $\mu_h = \frac{dI_{DS}}{dV_G} \times \frac{L}{WV_{DS}C_{EDL}}$ with L and W being the channel length and width (1.00×10^{-5} m and 4.90×10^{-1} m, respectively), V_{DS} is the source–drain voltage (V_{DS} = 50 mV), and C_{EDL} the electrical double layer capacitance extracted from the leakage current (C_{EDL}=5.756 µF cm^{-2}).

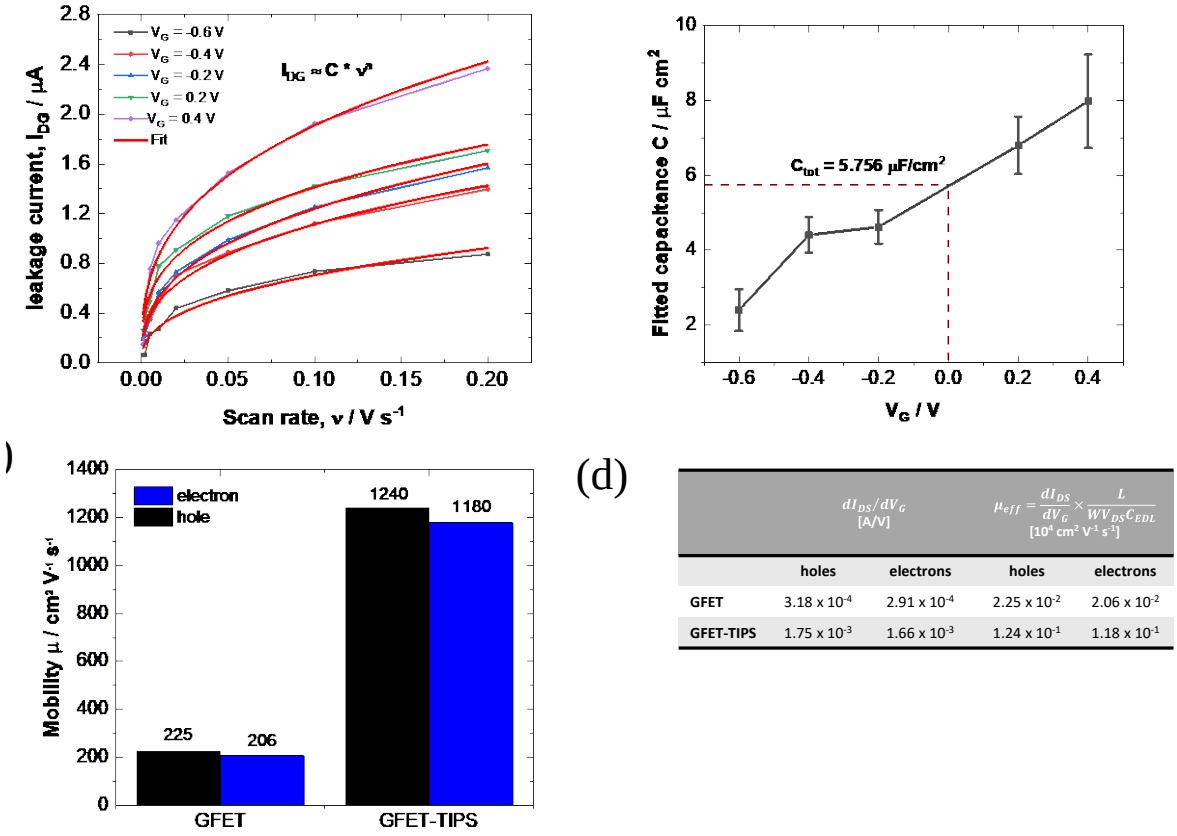

(d)

	dI_{DS}/dV_G [A/V]		$\mu_{eff} = \frac{dI_{DS}}{dV_G} \times \frac{L}{WV_{DS}C_{EDL}}$ [10^4 cm^2 V^{-1} s^{-1}]	
	holes	electrons	holes	electrons
GFET	3.18 x 10^{-4}	2.91 x 10^{-4}	2.25 x 10^{-2}	2.06 x 10^{-2}
GFET-TIPS	1.75 x 10^{-3}	1.66 x 10^{-3}	1.24 x 10^{-1}	1.18 x 10^{-1}

Figure S3: Determination of hole and electron mobility: (a) Leakage current vs. scan rate recorded at different applied VG. (b) Fitted capacitance vs. VG. (c) Electron and hole mobility of GFET and TIPS modified GFET. (d) Table summarizing hole and electron mobility values for GFET and GFET-TIPS.

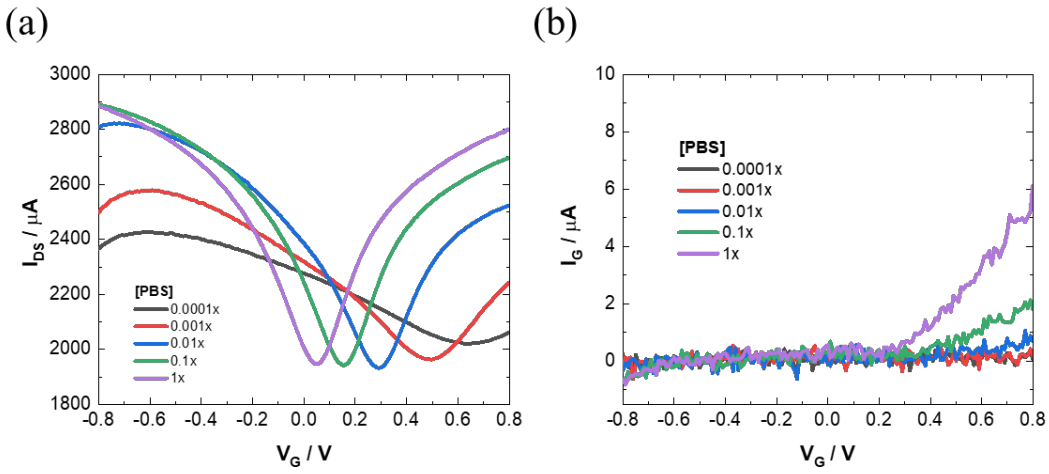

Figure S4: (a) Raw data of the EG-FET measurement including (b) leakage current (gate current). N=3.

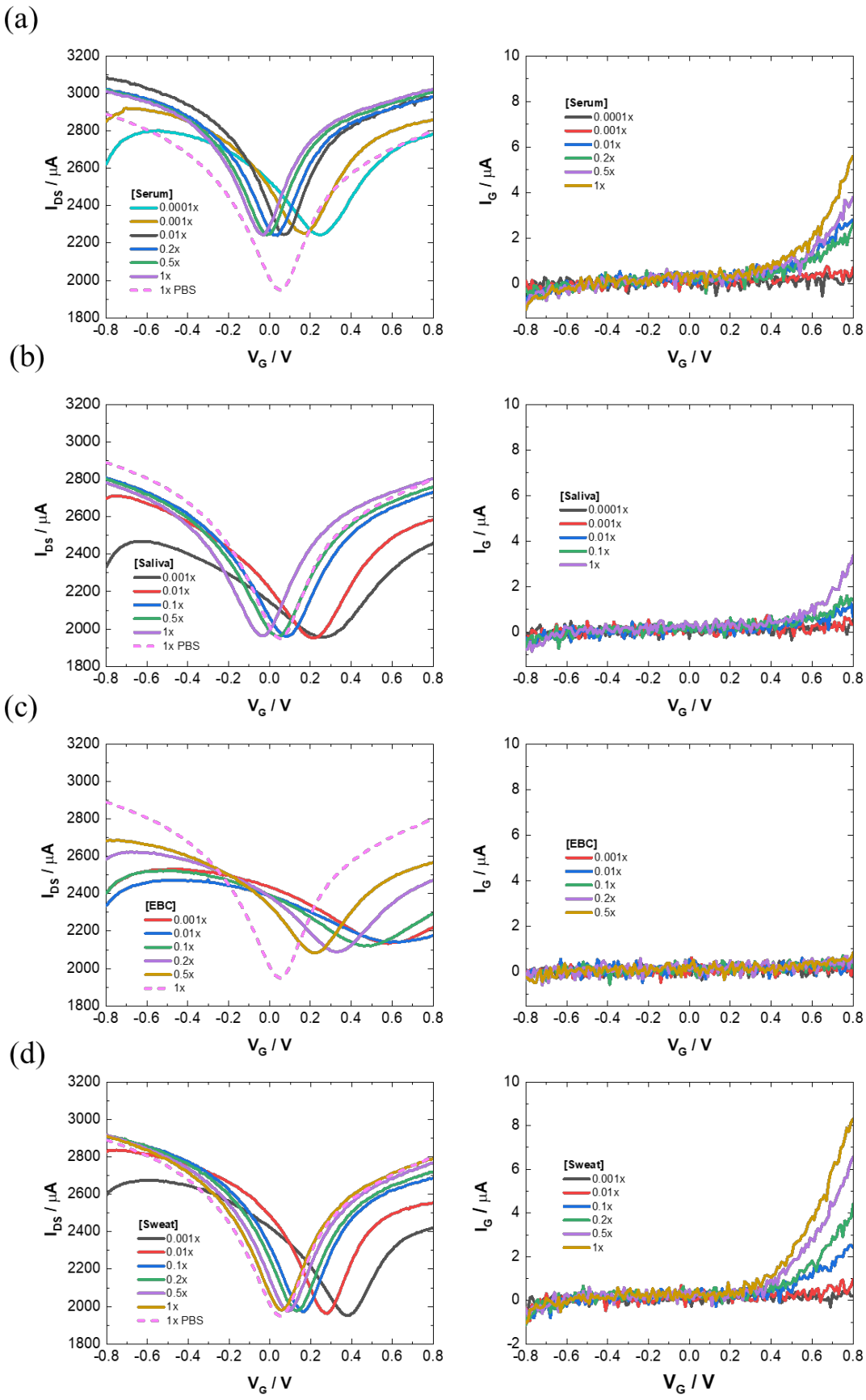

Figure S5: (a) Raw data of the EG-FET measurement including (b) leakage current (gate current).

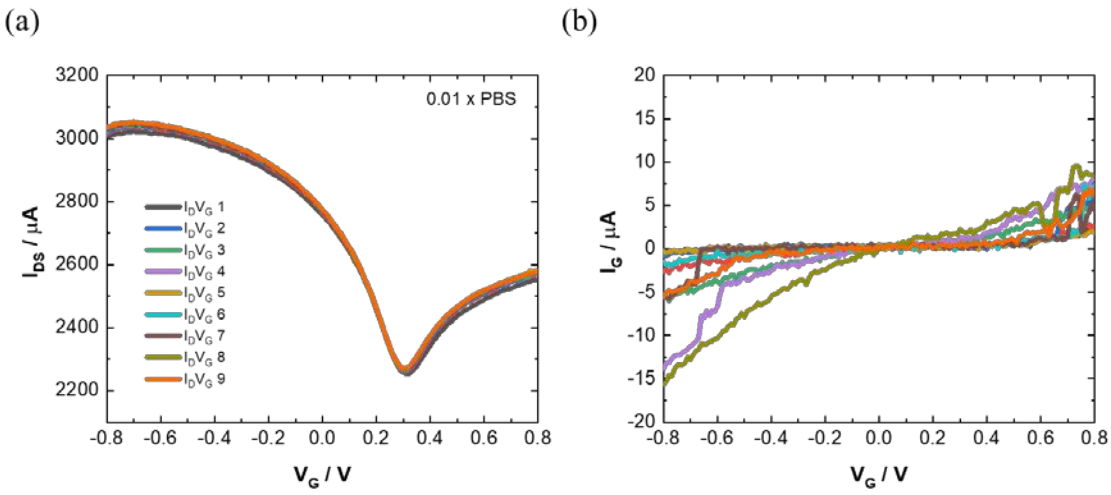

Figure S6: (a) Reproducibility of aptamer modified GFET transfer characteristics as determined from 9 fabricated devices. (b) leakage current (gate current).

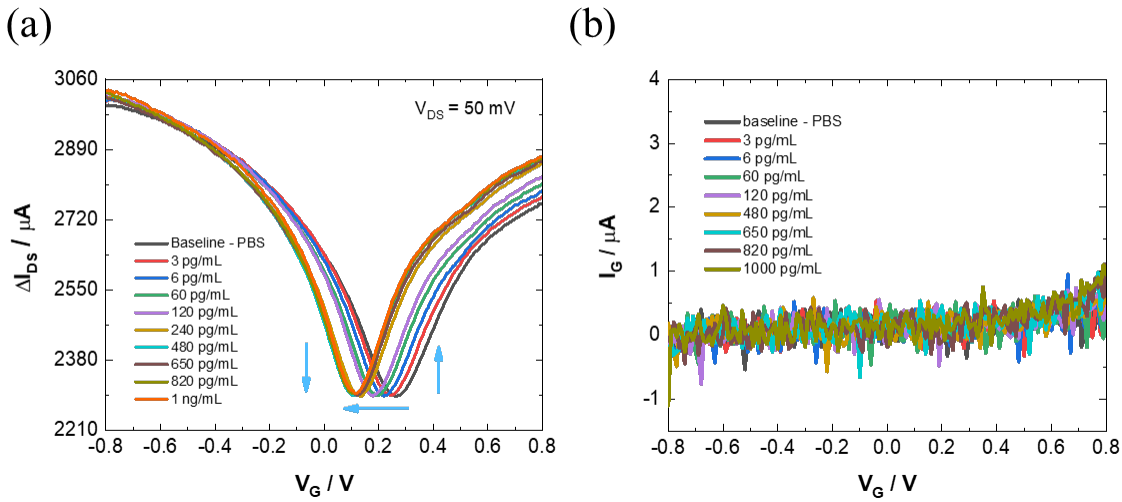

Figure S7: (a) cTnI-aptamer complex formation on GFET transfer characteristics with the respective leakage current (b).

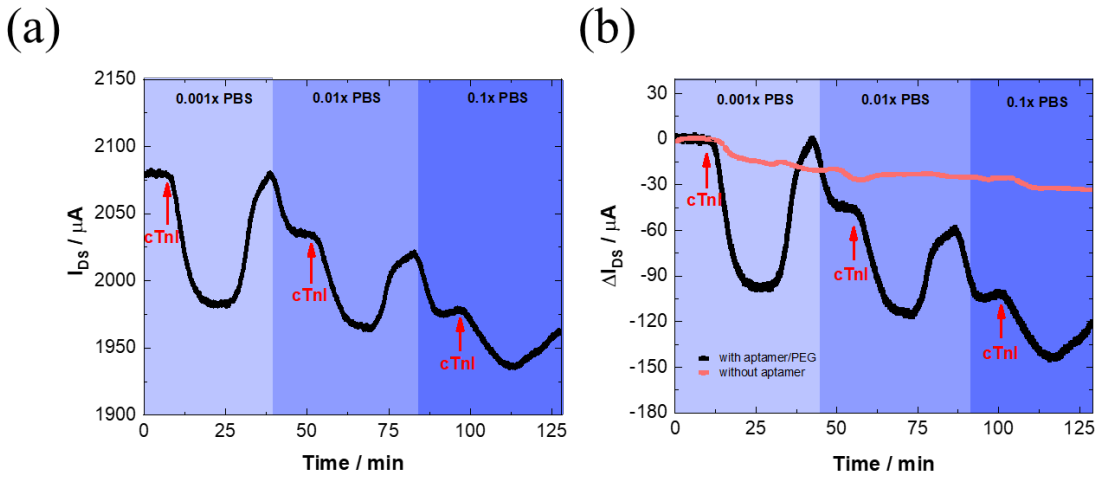

Figures S8: (a) Time-dependent measurements of 240 pg mL^{-1} cTnI in 0.001× PBS, 0.01× PBS and 0.1× PBS with regeneration after buffer washing. V_G = 350 mV (raw data). (b) Same as (a) with ΔI_{DS} = I_{DS}-StartingPoint(I_{DS}) and showing the control curve where cTnI was flushed over a GFET without aptamer immobilized.

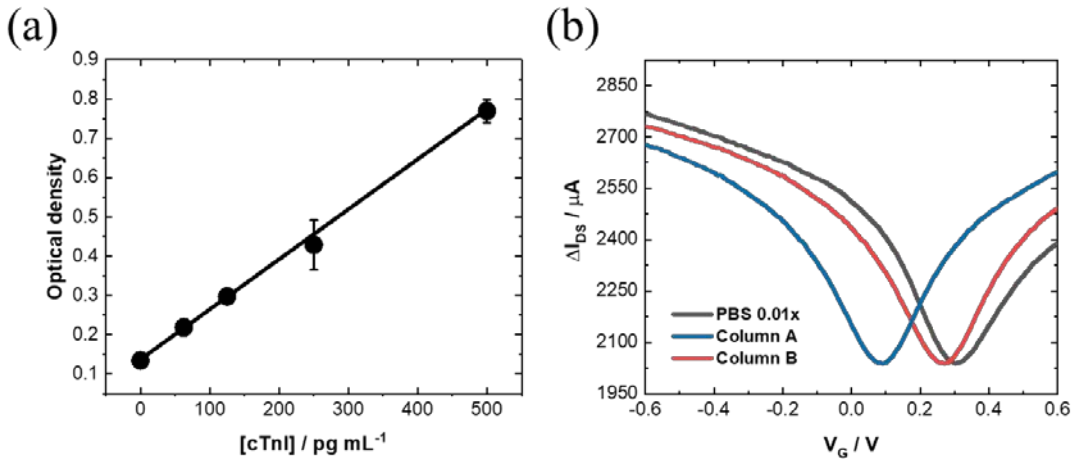

Figures S9: (a) Calibration curve of different cTnI concentrations from ELISA measurements. (b) Transfer characteristics of aptamer/PEG (2/1) modified GFET in 0.01× PBS (pH 7.4) and after desalination with columns A and B. V_{DS} = 50 mV.

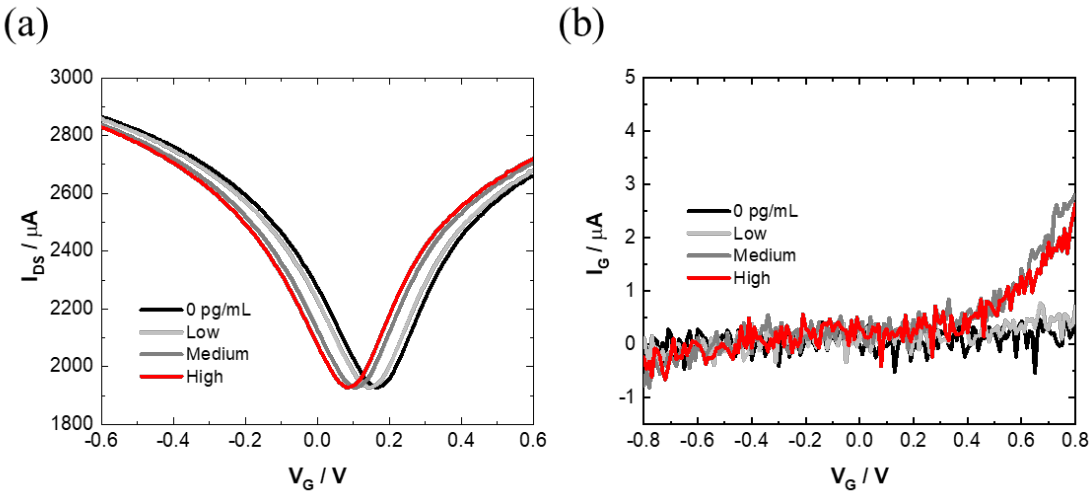

Figures S10: (a) cTnI-aptamer complex formation on GFET transfer characteristics with the respective leakage current (b).

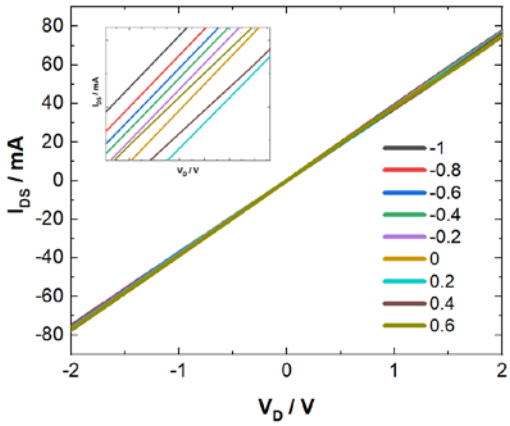

Figure S11: GFET output characteristics (I_DV_D) demonstrating the linearity of our device when using a source-drain voltage of 0.05 V.